

UNIVERSITY OF BIRMINGHAM

University of Birmingham
Research at Birmingham

Important role of forest disturbances in the global biomass turnover and carbon sinks

Pugh, Thomas; Arneth, Almut; Kautz, Markus; Poulter, Benjamin; Smith, Benjamin

DOI:

<https://doi.org/10.1038/s41561-019-0427-2>

License:

Other (please specify with Rights Statement)

Document Version

Peer reviewed version

Citation for published version (Harvard):

Pugh, T, Arneth, A, Kautz, M, Poulter, B & Smith, B 2019, 'Important role of forest disturbances in the global biomass turnover and carbon sinks', *Nature Geoscience*, vol. 12, pp. 730–735. <https://doi.org/10.1038/s41561-019-0427-2>

[Link to publication on Research at Birmingham portal](#)

Publisher Rights Statement:

Pugh, A. M. T. et al (2019) Important role of forest disturbances in the global biomass turnover and carbon sinks, *Nature Geoscience*, volume 12, pages 730–735, <https://doi.org/10.1038/s41561-019-0427-2>

This is an Accepted Manuscript version of an article published in *Nature Geoscience*.

General rights

Unless a licence is specified above, all rights (including copyright and moral rights) in this document are retained by the authors and/or the copyright holders. The express permission of the copyright holder must be obtained for any use of this material other than for purposes permitted by law.

- Users may freely distribute the URL that is used to identify this publication.
- Users may download and/or print one copy of the publication from the University of Birmingham research portal for the purpose of private study or non-commercial research.
- User may use extracts from the document in line with the concept of 'fair dealing' under the Copyright, Designs and Patents Act 1988 (?)
- Users may not further distribute the material nor use it for the purposes of commercial gain.

Where a licence is displayed above, please note the terms and conditions of the licence govern your use of this document.

When citing, please reference the published version.

Take down policy

While the University of Birmingham exercises care and attention in making items available there are rare occasions when an item has been uploaded in error or has been deemed to be commercially or otherwise sensitive.

If you believe that this is the case for this document, please contact UBIRA@lists.bham.ac.uk providing details and we will remove access to the work immediately and investigate.

1 **Biomass stocks in half of global forests controlled by large**
2 **disturbances**

3

4 Thomas A.M. Pugh^{1,2*}, Almut Arneth³, Markus Kautz⁴, Benjamin Poulter⁵ and
5 Benjamin Smith^{6,7}

6

7 ¹ School of Geography, Earth and Environmental Sciences, University of
8 Birmingham, Birmingham, B15 2TT, U.K.

9 ² Birmingham Institute of Forest Research, University of Birmingham,
10 Birmingham, B15 2TT, U.K.

11 ³ Karlsruhe Institute of Technology, IMK-IFU, 82467 Garmisch-Partenkirchen,
12 Germany.

13 ⁴ Department of Forest Health, Forest Research Institute Baden-Württemberg,
14 79100 Freiburg, Germany.

15 ⁵ Biospheric Sciences Laboratory, NASA Goddard Space Flight Center, Greenbelt,
16 MD 20771, U.S.A.

17 ⁶ Department of Physical Geography and Ecosystem Science, Lund University,
18 22362 Lund, Sweden.

19 ⁷ Hawkesbury Institute for the Environment, Western Sydney University, Penrith,
20 NSW 2751, Australia

21

22 * Corresponding author: t.a.m.pugh@bham.ac.uk

23

24

25 Forest disturbances leading to replacement of whole tree stands are a cornerstone
26 of forest dynamics, with drivers including fire, wind-throw, biotic outbreaks and
27 harvest. The frequency of disturbances may change over the next century,
28 impacting the age, composition and biomass of forests. However, the variation in
29 disturbance return time, i.e. the mean interval between disturbance events, across
30 the world's forested biomes remains poorly characterised, hindering
31 quantification of their role in the global carbon cycle. Here we present the global
32 distribution of stand-replacing disturbance return time inferred from satellite-
33 based observations of forest loss. Prescribing this distribution within a vegetation
34 model with a detailed representation of stand structure, we quantify the
35 importance of stand-replacing disturbances for biomass carbon turnover globally
36 over 2001-2014. Return time varied from less than 50 years in heavily-managed
37 temperate ecosystems to over 1000 years in tropical evergreen forests. Stand-
38 replacing disturbances accounted for 12.3% (95% confidence interval, 11.4-
39 13.7%) of annual biomass carbon turnover due to tree mortality globally, and in
40 44% of forested area biomass stocks are strongly sensitive to changes in
41 disturbance return time. Relatively small shifts in disturbance regimes in these
42 areas would substantially influence the forest carbon sink, that currently limits
43 climate change by offsetting emissions.

44

45 **Main text**

46

47 The amount of carbon stored in global forest biomass is similar to that in the
48 atmosphere¹, and, excluding the effects of land-use change, has been estimated to
49 have grown at *ca.* 1.5 PgC a⁻¹ over recent decades². This uptake has significantly

50 slowed the atmospheric growth rate of carbon dioxide and thus the rate of climate
51 change³. The accumulation of carbon in the stems of growing trees results from
52 the balance between the growth rates of vegetation and the average length of time
53 carbon remains in live biomass (hereafter, “biomass”), the turnover time,
54 calculated as the carbon stock divided by the flux of carbon loss through plant and
55 tissue death⁴. Quantification of this turnover time is crucial because it governs the
56 size of biomass stocks for a given growth rate and it is one of the most significant
57 uncertainties affecting projections of the terrestrial carbon cycle^{5,6}. Large-scale
58 estimates of carbon turnover times for whole ecosystems and for biomass have
59 been recently developed^{7,8}, but offer limited insight into the processes governing
60 biomass stocks because the turnover flux could only be approximated by
61 estimates of net primary productivity (NPP). This conflates turnover of soft
62 tissues, such as leaves and roots, with that of the woody carbon pools that
63 dominate biomass carbon stocks¹. To understand forest biomass turnover times
64 globally, large-scale tree mortality rates must be quantified.

65

66 Tree death is often the culmination of a prolonged period of physiological stress
67 related to a shortage of essential resources required for the synthesis of basic
68 metabolites, for instance, due to shading by other plants, low water availability, or
69 a shortage of soil nutrients such as N and P in plant-available forms^{9,10}.
70 Alternatively, disturbances such as wind-throw, fire, insect and disease outbreaks,
71 or anthropogenic activities such as wood harvest may constitute the cause of
72 death¹¹⁻¹⁶. Disturbances act on scales ranging from a single tree to whole forest
73 stands or landscapes. Here we investigate stand-replacing disturbances, defined
74 operationally as discrete events resulting in the death of all, or almost all, living

75 tree biomass at a scale of 0.1 ha or larger. Such events affect the average tree age
76 as well as the stature, density and composition of forest stands^{11,17}, in turn
77 impacting carbon storage¹⁸. There is evidence that the frequency of disturbances
78 may be changing globally, with continued change likely in the future^{8,13-15,19,20}. Yet,
79 to understand the consequences of future changes, it is first necessary to provide
80 a baseline of current conditions. Such a baseline is lacking for stand-replacing
81 disturbances across global forests.

82

83 **The frequency of stand-replacing disturbances.** We estimated the frequency of
84 stand-replacing disturbances across all global forests at 1° spatial resolution.
85 Drawing on a Landsat-based (2000-2014) forest-loss product²¹, we performed a
86 space-for-time substitution, calculating the disturbance rotation period, τ , defined
87 as the mean time period for the area disturbed to equal the area of the grid cell¹¹,

88
$$\tau_i = \frac{A_{T,i}}{\overline{A_{L,i}} - \overline{A_{C,i}}} \quad (1)$$

89 where i is a grid-cell index, A_T is total forest area in that 1° x 1° grid cell, $\overline{A_L}$ the
90 annual mean total forest loss over 2000-2014 calculated based on all Landsat-
91 pixels within the grid cell and $\overline{A_C}$ the annual mean forest loss due to conversion to
92 a non-forest land-use type (Methods). This observation-based τ is referred to as
93 τ_0 . While rare disturbances may be undersampled for individual grid cells, this is
94 less of an issue across a neighbourhood of many grid cells, and the global-scale
95 pattern is expected to be robust (Suppl. Note 1). We take τ as indicative of the
96 typical or average disturbance return time from all causes at any location in a grid
97 cell, reflecting causes such as wood harvest, as well as natural disturbances such
98 as fires, large-scale wind-throws and biotic outbreaks. Whilst the drivers of each

99 of these disturbance agents differ markedly, their consequences for carbon
100 turnover in live biomass are assumed to be similar at large scales. Disturbances
101 associated with the conversion of forests to other land-uses were explicitly
102 excluded (Methods), allowing us to focus on dynamics within closed-canopy
103 forests .

104

105 Disturbance return time varies substantially across the global forest area (Fig. 1a).
106 The stand-replacing disturbances quantified here are more common in needleleaf
107 and mixed forests (median τ_0 of *ca.* 300 years) than they are in temperate or
108 tropical broadleaf forests (median τ_0 of 830 to more than 1000 years), however
109 forest type emerges as a poor predictor of the spatial distribution of τ_0 (Fig. 1c).
110 In large areas of forest, stand-replacing disturbances are actually very rare events;
111 35% of forest area experienced stand-replacing disturbances with an average
112 frequency equivalent to less than once every thousand years. In these forests the
113 vast majority of tree mortality must thus be non-stand-replacing. The 95%
114 confidence intervals for τ_0 typically span a range less than one third of the
115 absolute value of τ_0 , except in areas of substantial land-use change (Fig. 1b, Suppl.
116 Fig. 7).

117

118 We compared our results against an inventory-based compilation of forest stand
119 age (GFADv1.1²²). Despite the different scale and characteristics of inventory data
120 we found qualitative consistency in tropical evergreen and boreal forests, as well
121 as some regions under intensive forest management, but also suggestions of a
122 substantial amount of disturbance in some temperate forests below the scale
123 captured in the Landsat data and of legacies of past afforestation (Suppl. Note 2,

124 Suppl. Fig. 1). We also found consistency between our results and previous studies
125 of disturbance frequencies in the tropics^{17,23,24} and Canada²⁵ (Suppl. Note 3; Suppl.
126 Fig. 2), and biotic outbreak disturbances in the U.S.A.²⁶ (Suppl. Note 3; Suppl. Fig.
127 3).

128

129 **Influence of stand-replacing disturbances on the carbon cycle.** We apply the
130 gridded estimates of τ_0 within a dynamic global vegetation model (DGVM) with an
131 explicit representation of forest stand structural development. τ was kept
132 constant in each grid cell for the entire model simulation, calculating the pseudo-
133 equilibrium effect of τ_0 on forest dynamics. Stand-replacing disturbances are
134 simulated to dominate overall tree mortality, and associated carbon turnover,
135 across large areas of the mid-latitude and boreal forests, accounting for over 60%
136 in some locations, but are not the dominant cause of mortality in most tropical
137 forests (Fig. 2a,b).

138

139 The total turnover of biomass carbon as a result of stand-replacing disturbances
140 at pseudo-equilibrium in our simulations is 1.00 (95% confidence interval, 0.91-
141 1.11) PgC a⁻¹, equivalent to 4.4 (4.0-4.9) % of total biomass carbon turnover in
142 closed-canopy forests (i.e. including soft-tissue turnover) (Fig. 2b,c). These
143 numbers are supported by an empirical cross-check based on satellite-derived
144 NPP and biomass estimates which combined satellite LIDAR and radar
145 observations with ground-based reference plots (red dots in Fig. 2b,c; Methods).
146 The fraction of biomass carbon turnover due to mortality must be taken with
147 caution, however, until biomass turnover rates from other forms of mortality can

148 be fully constrained. Likewise the total turnover flux is dependent on accurate
149 calculation of global biomass stocks, which remain uncertain¹.

150

151 The tropical broadleaved evergreen forest type provides the largest contribution
152 to global biomass carbon turnover from stand-replacing disturbances, followed by
153 needleleaved evergreen forest (Fig. 2c). Although stand-replacing disturbances
154 are infrequent in tropical evergreen forest, the disturbance-related flux is
155 significant, as the amount of biomass in these forests is very high compared to
156 elsewhere²⁷⁻³⁰. Conversely, low τ will tend to suppress biomass stocks, limiting
157 the turnover flux generated in each disturbance event. Our estimates of biomass
158 carbon losses for tropical evergreen forest will tend towards the upper limit of
159 uncertainty because τ_0 was capped at 1000 years for reasons of sampling
160 (Methods); disturbance return times could in fact be even longer in some parts of
161 the tropics³¹. However, as demonstrated below, the sensitivity of biomass to very
162 high τ is low. Different disturbance agents cannot be distinguished in our data, but
163 carbon emissions from wildfire taken from the GFED dataset³² summed over the
164 same global forest area give a mean of 0.12 Pg C a⁻¹ over 2000-2014 (Methods),
165 suggesting that fires are globally a relatively minor driver of stand-replacing
166 disturbances in closed-canopy forests.

167

168 **Sensitivity of forest biomass to disturbance return time.** We ascertain the
169 influence on ecosystem properties of possible changes in τ , or errors in its
170 determination, for a randomly-selected grid cell from each of the tropical,
171 temperate and boreal zones. For each grid cell we run 100 individual simulations
172 varying τ sequentially within a plausible range of 10 to 1000 years. The resultant

173 range in pseudo-equilibrium carbon stocks reflects variation in τ alone,
174 independent of other environmental conditions or vegetation attributes (in
175 particular that the resilience of vegetation to disturbance does not change with τ).
176 The resulting curve of biomass carbon versus τ shows two distinct regimes (Fig.
177 3a); a regime of strong sensitivity of biomass to τ when τ is low, and a weak
178 sensitivity regime when τ is high. These regimes result from shifts in the primary
179 cause of dominant tree death. With low τ the majority of trees die from stand-
180 replacing disturbance before they get old enough to die from another cause. Thus,
181 τ emerges as the primary limit on simulated stand biomass across almost all
182 stands. In contrast, when τ is large most canopy trees die from causes other than
183 stand-replacing disturbances. In this case, τ is not a primary limit on simulated
184 stand maximum biomass and changes in τ will only affect a subset of stands across
185 the landscape at any time.

186

187 To map the sensitivity of forests to changes in τ globally we propose a new metric
188 based on a fractional reduction of τ_0 . Plotting τ_0 against the difference in simulated
189 biomass between global simulations run with τ_0 and $0.5\tau_0$ reveals a similar curve
190 to the site-based simulations (Fig. 3b). We categorise global forests into two
191 classes of sensitivity to disturbances: where the biomass under $0.5\tau_0$ is less than
192 90% of that under τ_0 , the forest is classified as having strong sensitivity to changes
193 in τ (i.e. stand-replacing disturbance frequency is a strong control on biomass),
194 with other areas having weak sensitivity (i.e. other forms of mortality control
195 biomass). The τ_0 at which this sensitivity threshold, $\tau_{crit,90}$, is crossed varies with
196 forest type, with a global average of 444 (429-457) years. This implies a mean
197 recovery time of 222 years (i.e. $0.5\tau_{crit,90}$) to 90% of biomass stocks under τ_0 . This

198 is substantially longer than the 66 years reported for regain 90% of old-growth
199 biomass in individual tropical forest stands³³ and follows because our simulations
200 take account of succession and also scale one stage further to the net landscape
201 change in biomass. I.e. individual stands may recover rapidly, but across the
202 landscape more stands are in a recently-disturbed state. Overall, 44 (39-49) % of
203 global forest falls into the strongly sensitive category, with 23 (20-27) % falling
204 into a very strong sensitivity category in which halving τ_0 leads to biomass
205 dropping below 80% of that under τ_0 ($\tau_{crit,80}$). Forests in weak-sensitivity τ
206 regimes are particularly located in tropical and temperate zones.(Fig. 3c).

207

208 The biomass content of weak-sensitivity forests would still be vulnerable to very
209 large reductions in τ , for instance through a catastrophic shift to an entirely new
210 disturbance regime³⁴ or introduction of a new disturbance type³⁵, but is robust to
211 moderate changes in τ . This is demonstrated in additional simulations using τ_0
212 adjusted up or down by a factor of up to 4; weak-sensitivity forests show large
213 biomass changes only with substantial reductions in τ , whereas high-sensitivity
214 forests show a steep relationship with τ (Fig. 3d). These results were robust to
215 assumptions on the type of disturbance (shaded areas in Fig. 3d), although we
216 note that selective effects of disturbance type on species composition^{35,36}, and thus
217 potentially on biomass and turnover³⁷, could only be treated crudely within the
218 plant functional type classes used for global simulation and there may be non-
219 linear shifts not accounted for in the model³⁸. The time taken for forest biomass to
220 approach a new pseudo-equilibrium state will depend on the new value of τ to
221 which the ecosystem is subjected. In general, changes in τ will only be fully

222 reflected in carbon fluxes over the next century if that new τ is of the order of 100
223 years or less.

224

225 Unlike the influence of τ on biomass (Fig. 3d), its influence on soil carbon stocks is
226 strongly sensitive to the rate of decomposition of the resulting litter and soil
227 organic matter, and also depends on biomass removals, for instance in conjunction
228 with wood harvest (Fig. 3e). When disturbed biomass is transferred to the litter,
229 disturbance only has notable negative consequences when τ becomes very low,
230 reducing the fraction of longer-lived woody biomass entering the litter. However,
231 harvest removals or burning of biomass substantially reduce the input rate of
232 carbon to the soil, leading to a strong positive relationship between soil carbon
233 density and τ . This strong sensitivity of soil carbon storage to the type, as well as
234 the frequency, of disturbance, underlines the need for improved discrimination of
235 different disturbance types at the global scale³⁹. Response times for soil will lag
236 those for vegetation, and be influenced by the form of necromass left after
237 disturbance⁴⁰, another area of high process uncertainty. Summing over both
238 vegetation and soil, a widespread shift in disturbance regimes equivalent to a
239 halving of τ_0 across all closed-canopy forests would ultimately release 47-80 Pg C,
240 depending on the form of that disturbance, while an increase in time between
241 disturbances could promote carbon uptake (Suppl. Fig. 10).

242

243 **Concluding remarks.** The results of this study allow us to partition one important
244 component of overall biomass turnover rates in global forests^{1,8}. Although stand-
245 replacing disturbances constitute a relatively small portion of the overall global
246 biomass turnover flux, small changes in τ would exert a strong influence on

247 biomass stocks in almost half of the world's forests. DGVMs and land-surface
248 models currently incorporating explicit representations of forest demography⁴¹
249 must properly account for stand-replacing disturbances to avoid biases in net
250 carbon uptake or erroneous calibration of processes to account for these biases.
251 Our study highlights the importance of accounting for variability in forest
252 disturbance regimes, yet constitutes only a first step; 88% of global carbon
253 turnover due to tree mortality is not explained by stand-replacing disturbances. It
254 thus remains crucial to constrain other causes of mortality, including disturbances
255 below stand-scale^{23,42}, drought⁴³, and demography. High-resolution data from
256 satellites, along with forest inventories, will be key in this regard.

257

258 Our results provide a snapshot of a global stand-replacing disturbance pattern
259 that may be undergoing rapid change¹³⁻¹⁵. Drivers of such change, whether
260 climate, management or otherwise are uncertain and likely highly region-
261 specific^{13-16,19,20}. Future work must consider how carbon emissions through
262 changes in τ are likely to interact with other aspects of environmental change,
263 such as the fertilising effects of rising CO₂ concentrations, which may reduce
264 vulnerability to disturbance⁴⁴, as well as seeking to close the feedback loops
265 between disturbances, climate and vegetation properties. Changing disturbances
266 could both augment and offset carbon loading of the atmosphere caused by
267 anthropogenic carbon emissions³; better understanding the role of forest
268 disturbances in the carbon cycle is therefore highly relevant to the assessment of
269 emissions reductions necessary to meet climate targets.

270

271 **References**

- 272 1. Erb, K. et al. Unexpectedly large impact of forest management and grazing
273 on global vegetation biomass. *Nature* **553**, 73–76 (2018).
- 274 2. Pan, Y. et al. A large and persistent carbon sink in the world's forests.
275 *Science* **333**, 988–93 (2011).
- 276 3. Quéré, C. Le et al. Global Carbon Budget 2017. *Earth Syst. Sci. Data* **10**,
277 405–448 (2018).
- 278 4. Sierra, C. A., Müller, M., Metzler, H., Manzoni, S. & Trumbore, S. E. The
279 muddle of ages, turnover, transit, and residence times in the carbon cycle.
280 *Glob. Chang. Biol.* **23**, 1763–1773 (2017).
- 281 5. Friend, A. D. et al. Carbon residence time dominates uncertainty in
282 terrestrial vegetation responses to future climate and atmospheric CO₂.
283 *Proc. Natl. Acad. Sci. U. S. A.* **111**, 3280–3285 (2014).
- 284 6. Ahlström, A., Xia, J., Arneeth, A., Luo, Y. & Smith, B. Importance of
285 vegetation dynamics for future terrestrial carbon cycling. *Environ. Res.*
286 *Lett.* **10**, 054019 (2015).
- 287 7. Carvalhais, N. et al. Global covariation of carbon turnover times with
288 climate in terrestrial ecosystems. *Nature* **514**, 213–217 (2014).
- 289 8. Erb, K.-H. et al. Biomass turnover time in terrestrial ecosystems halved by
290 land use. *Nat. Geosci.* **9**, 674–678 (2016).
- 291 9. Waring, R. H. Characteristics of Trees Predisposed to Die. *BioScience* **37**,
292 569–574 (1987).
- 293 10. McDowell, N. G. et al. The interdependence of mechanisms underlying
294 climate-driven vegetation mortality. *Trends Ecol. Evol.* **26**, 523–532
295 (2011).

- 296 11. Pickett, S. T. A. & White, P. S. *The ecology of natural disturbances and patch*
297 *dynamics*. (Academic Press Inc, Orlando, 1985).
- 298 12. Frohling, S. et al. Forest disturbance and recovery: A general review in the
299 context of spaceborne remote sensing of impacts on aboveground
300 biomass and canopy structure. *J. Geophys. Res.* **114**, G00E02 (2009).
- 301 13. Kurz, W., Stinson, G., Rampley, G., Dymond, C. & Neilson, E. Risk of natural
302 disturbances makes future contribution of Canada's forests to the global
303 carbon cycle highly uncertain. *Proc. Natl. Acad. Sci. U. S. A.* **105**, 1551–
304 1555 (2008).
- 305 14. Seidl, R., Schelhaas, M.-J., Rammer, W. & Verkerk, P. J. Increasing forest
306 disturbances in Europe and their impact on carbon storage. *Nat. Clim.*
307 *Chang.* **4**, 806–810 (2014).
- 308 15. Flannigan, M., Stocks, B., Turetsky, M. & Wotton, M. Impacts of climate
309 change on fire activity and fire management in the circumboreal forest.
310 *Glob. Chang. Biol.* **15**, 549–560 (2009).
- 311 16. Hurtt, G. C. et al. Harmonization of land-use scenarios for the period
312 1500–2100: 600 years of global gridded annual land-use transitions,
313 wood harvest, and resulting secondary lands. *Clim. Change* **109**, 117–161
314 (2011).
- 315 17. Cole, L. E. S., Bhagwat, S. A. & Willis, K. J. Recovery and resilience of
316 tropical forests after disturbance. *Nat. Commun.* **5**, 1–7 (2014).
- 317 18. Pregitzer, K. S. & Euskirchen, E. S. Carbon cycling and storage in world
318 forests: biome patterns related to forest age. *Glob. Chang. Biol.* **10**, 2052–
319 2077 (2004).

- 320 19. Seidl, R. et al. Forest disturbances under climate change. *Nat. Clim. Chang.*
321 **7**, 395–402 (2017).
- 322 20. Reyser, C. P. O. et al. Are forest disturbances amplifying or canceling out
323 climate change-induced productivity changes in European forests?
324 *Environ. Res. Lett.* **12**, 034027 (2017).
- 325 21. Hansen, M. C. et al. High-resolution global maps of 21st-century forest
326 cover change. *Science* **342**, 850–853 (2013).
- 327 22. Poulter, B. et al. *The global forest age dataset and its uncertainties*
328 *(GFADv1.1)*. (2019). doi.pangaea.de/10.1594/PANGAEA.897392
- 329 23. Espírito-Santo, F. D. B. et al. Size and frequency of natural forest
330 disturbances and the Amazon forest carbon balance. *Nat. Commun.* **5**,
331 3434 (2014).
- 332 24. Chambers, J. Q. et al. The steady-state mosaic of disturbance and
333 succession across an old-growth Central Amazon forest landscape. *Proc.*
334 *Natl. Acad. Sci. U. S. A.* **110**, 3949–3964 (2013).
- 335 25. White, J. C., Wulder, M. A., Hermosilla, T., Coops, N. C. & Hobart, G. W. A
336 nationwide annual characterization of 25 years of forest disturbance and
337 recovery for Canada using Landsat time series. *Remote Sens. Environ.* **194**,
338 303–321 (2017).
- 339 26. Kautz, M., Meddens, A. J. H., Hall, R. J. & Arneth, A. Biotic disturbances in
340 Northern Hemisphere forests – a synthesis of recent data, uncertainties
341 and implications for forest monitoring and modelling. *Glob. Ecol. Biogeogr.*
342 **26**, 533–552 (2017).
- 343 27. Avitabile, V. et al. An integrated pan-tropical biomass map using multiple
344 reference datasets. *Glob. Chang. Biol.* **22**, 1406–1420 (2016).

- 345 28. Santoro, M. et al. Remote Sensing of Environment Forest growing stock
346 volume of the northern hemisphere: Spatially explicit estimates for 2010
347 derived from Envisat ASAR. *Remote Sens. Environ.* **168**, 316–334 (2015).
- 348 29. Avitabile, V. et al. Comparative analysis and fusion for improved global
349 biomass mapping. in *Global Vegetation Monitoring and Modeling 3 – 7*
350 *February 2014, Avignon (France)* (2014).
- 351 30. Thurner, M. et al. Carbon stock and density of northern boreal and
352 temperate forests. *Glob. Ecol. Biogeogr.* **23**, 297–310 (2014).
- 353 31. Espírito-Santo, F. D. B. et al. Storm intensity and old-growth forest
354 disturbances in the Amazon region. *Geophys. Res. Lett.* **37**, L11403 (2010).
- 355 32. van der Werf, G. R. et al. Global fire emissions estimates during 1997-
356 2016. *Earth Syst. Sci. Data* **9**, 697–720 (2017).
- 357 33. Poorter, L. et al. Biomass resilience of Neotropical secondary forests.
358 *Nature* **530**, 211–214 (2016).
- 359 34. Scheffer, M., Carpenter, S., Foley, J. A., Folke, C. & Walker, B. Catastrophic
360 shifts in ecosystems. *Nature* **413**, 591–6 (2001).
- 361 35. Johnstone, J. F. et al. Changing disturbance regimes, ecological memory,
362 and forest resilience. *Front. Ecol. Environ.* **14**, 369–378 (2016).
- 363 36. Marra, D. M. et al. Large-scale wind disturbances promote tree diversity in
364 a Central Amazon forest. *PLoS One* **9**, e103711 (2014).
- 365 37. Marra, D. M. et al. Predicting biomass of hyperdiverse and structurally
366 complex central Amazonian forests – a virtual approach using extensive
367 field data. *Biogeosciences* **13**, 1553–1570 (2016).
- 368 38. Marra, D. M. et al. Windthrows control biomass patterns and functional
369 composition of Amazon forests. *Glob. Chang. Biol.* **24**, 5867–5881 (2018).

- 370 39. McDowell, N. G. et al. Global satellite monitoring of climate-induced
371 vegetation disturbances. *Trends Plant Sci.* **20**, 114–123 (2015).
- 372 40. Renninger, H. J., Carlo, N., Clark, K. L. & Schäfer, K. V. R. Modeling
373 respiration from snags and coarse woody debris before and after an
374 invasive gypsy moth disturbance. *J. Geophys. Res. Biogeosciences* **119**,
375 630–644 (2014).
- 376 41. Fisher, R. A. et al. Vegetation demographics in Earth System Models: A
377 review of progress and priorities. *Glob. Chang. Biol.* **24**, 35–54 (2018).
- 378 42. Marvin, D. C. & Asner, G. P. Branchfall dominates annual carbon flux
379 across lowland Amazonian forests. *Environ. Res. Lett.* **11**, 094027 (2016).
- 380 43. Allen, C. D., Breshears, D. D. & McDowell, N. G. On underestimation of
381 global vulnerability to tree mortality and forest die-off from hotter
382 drought in the Anthropocene. *Ecosphere* **6**, 129 (2015).
- 383 44. Dolan, K. A. et al. Disturbance Distance: quantifying forests' vulnerability
384 to disturbance under current and future conditions. *Environ. Res. Lett.* **12**,
385 114015 (2017).

386

387 Correspondence and requests for materials should be addressed to T. A. M. Pugh,

388 t.a.m.pugh@bham.ac.uk.

389

390 **Acknowledgements**

391

392 TAMP acknowledges funding from the European Research Council (ERC) under
393 the European Union's Horizon 2020 research and innovation programme (grant
394 agreement No 758873, TreeMort). TAMP, AA and MK acknowledge support from

395 EU FP7 grant LUC4C (grant no. 603542), and the Helmholtz Association in its
396 ATMO programme and its impulse and networking fund. This is paper number 36
397 of the Birmingham Institute of Forest Research. BS acknowledges funding from
398 the Swedish Research Council FORMAS, the Strategic Research Area BECC and the
399 Lund University Centre for Studies of Carbon Cycle and Climate Interactions
400 (LUCCI). BP was supported by the NASA Terrestrial Ecology program. Stijn
401 Hantson, Sally Archibald, Jon Sadler, Tom Matthews and Sergei Petrovskii are
402 thanked for discussions which helped improve the manuscript, as are Mike
403 Wulder for providing the Canadian ecozones mask, Emma Ferranti for help with
404 file conversion and Veiko Lehsten for assistance with the data deposition.

405

406 **Author contributions**

407

408 TP conceived and designed the study with contributions from AA and BS. BP and
409 MK contributed data. TP carried out the model simulations. TP led the analysis
410 and wrote the paper with contributions from all authors.

411

412 **Competing financial interests**

413

414 The authors declare no competing financial interests.

415

416 Figure 1. **Forest disturbance rotation periods. a**, τ_0 calculated over 2000-2014.
417 **b**, Uncertainty in τ_0 , displayed as the difference between the 95% confidence
418 intervals divided by the central estimate. Uncertainty values of zero reflect 95%
419 confidence that τ_0 is over 1000 years. **c**, Boxplot of τ_0 grouped by forest type (see
420 Methods for codes). Circles show the median value, black triangles the 95%
421 confidence limits of the median, thick lines the interquartile range and whiskers
422 extend to a maximum of 1.5 times the interquartile range. Numbers indicate the
423 number of grid cells for each forest type.

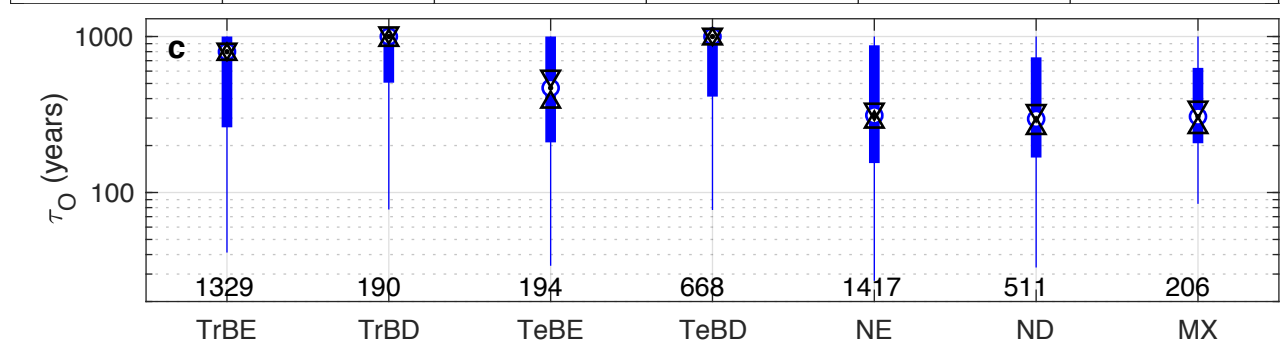
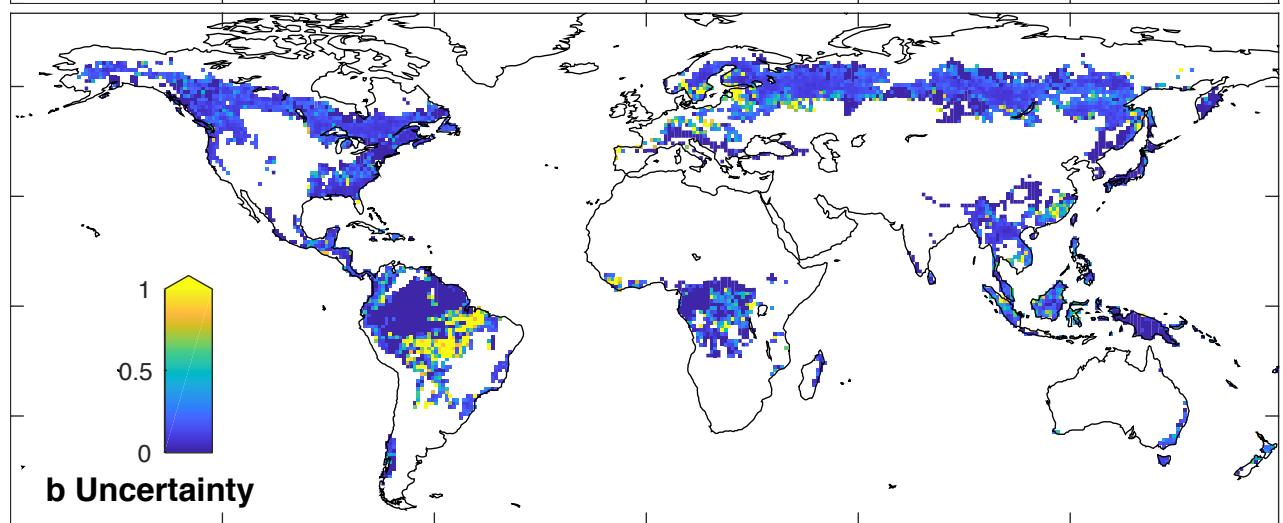
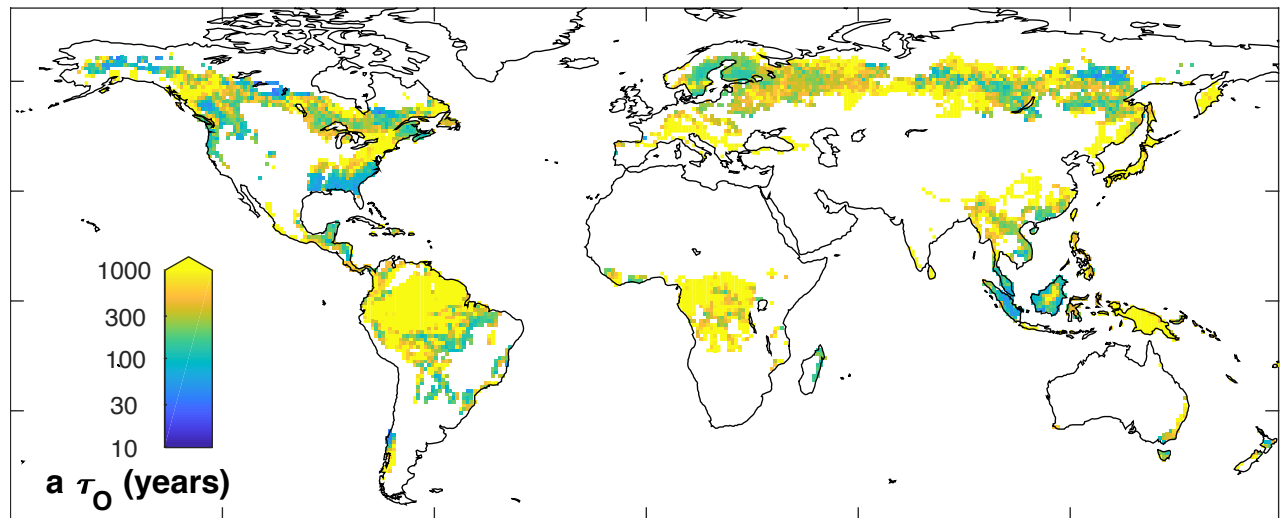
424

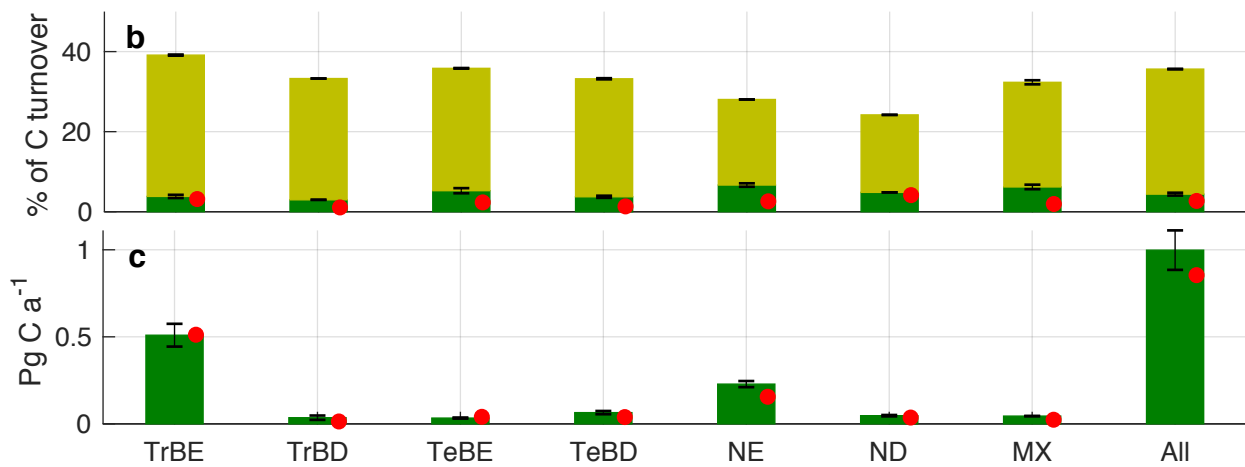
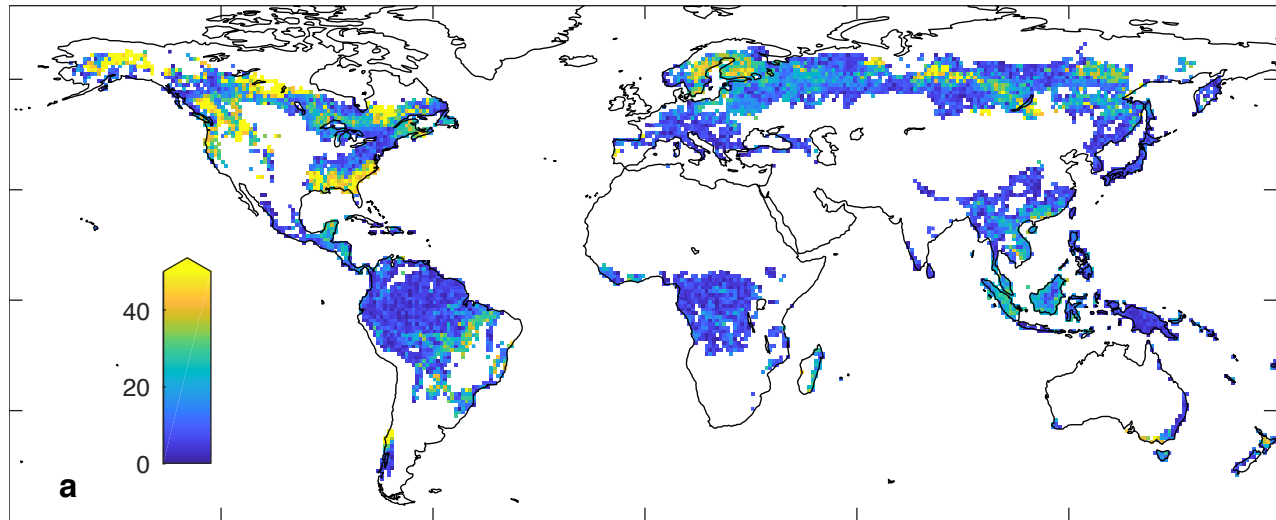
425 Figure 2. **Carbon turnover fluxes from closed-canopy forest for 2001-2014. a**,
426 Fraction of carbon turnover fluxes resulting from vegetation mortality due to
427 stand-replacing disturbances (colour scale capped at 50%), calculated using τ_0 to
428 drive LPJ-GUESS. Breakdown by forest type of: **b**, fraction of carbon turnover
429 fluxes resulting from vegetation mortality (whole bars) and from stand-replacing
430 disturbances (darker shading); **c**, total turnover flux of vegetation carbon due to
431 stand-replacing disturbance. Error bars show the range of simulations driven by
432 the 95% confidence intervals of τ_0 . Red dots show results from an observationally-
433 based cross-check method (Methods). Forest types as in Fig. 1.

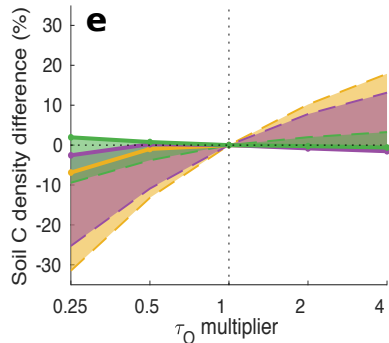
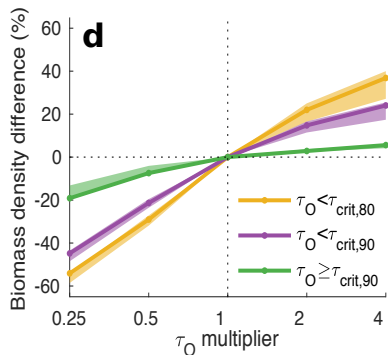
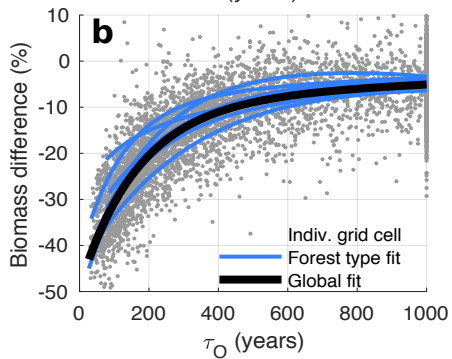
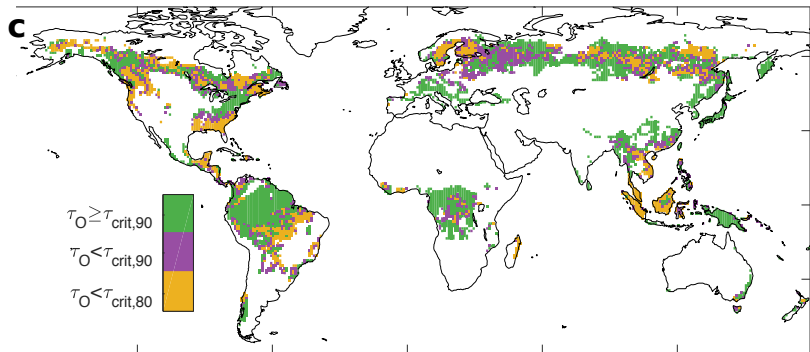
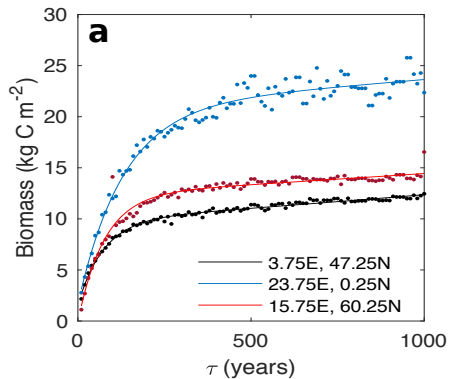
434

435 Figure 3. **Sensitivity of biomass to changes in τ . a**, Simulated biomass versus τ
436 for three random forested locations. Dots show individual simulations and lines a
437 fitted exponential function. **b**, Sensitivity to τ_0 of difference in simulated biomass
438 between simulations with τ_0 and $0.5\tau_0$. **c**, Sensitivity of biomass carbon stocks to
439 changes in τ . Shading indicates the sensitivity regime. **d, e**, Effect of multiplicative
440 perturbation in τ on vegetation and soil carbon density averaged across the

441 different sensitivity classes. Shaded areas show range of sensitivity simulations
442 testing assumptions on the type of disturbance assumed (solid lines for standard
443 simulation) (Methods).
444







445

446 **Methods**

447

448 **Calculation of τ_0 .** τ_0 was calculated as defined in Eq. 1. We first created a forest
449 mask by aggregating year 2000 forest canopy cover data at 0.00025° (ca. 30 m)
450 resolution²¹ to 0.01° resolution. Grid cells with at least 50% canopy cover at 0.01°
451 resolution were assigned as closed-canopy forest. Further aggregation then
452 provided the fractional coverage of closed-canopy forest at 1° resolution (A_T).
453 Across each 1° grid cell we then summed up the total area of 0.00025° pixels which
454 underwent forest loss during 2000-2014 and were located within the 0.01° grid
455 cells assigned as closed-canopy forest. A grid cell could only be counted as lost
456 once during the period. Dividing this sum by the length of the 14 year observation
457 period provided $\overline{A_L}$. A threshold of 25% forest cover at the 1° grid cell level was
458 used throughout this study in order to provide sufficient statistical power for
459 calculation of τ_0 . The total forested area meeting these conditions is 2.71×10^7
460 km^2 . Fig. 1c was calculated from the gridded τ_0 estimate using the "boxplot"
461 function of Matlab® 2014b.

462

463 This above definition provides a calculation of τ as a function of forest area. An
464 alternative definition of τ would be to define it relative to canopy area. In this case
465 A_T would be the total canopy area within the 0.01° grid cells designated as closed
466 canopy forest, making use of the fractional canopy cover metric provided by
467 Hansen *et al.*²¹, and $\overline{A_L}$ would be the sum of pixels undergoing forest loss
468 multiplied by the fractional canopy cover of those pixels before disturbance. Using
469 this canopy-area definition slightly reduces our estimates of τ_0 in most locations

470 (Suppl. Fig. 4), but the forest-area definition is preferred as it recognises that
471 whilst disturbances reduce canopy cover, they do not reduce the area of forest
472 unless associated with a land-use change.

473

474 Forest losses due to land-use change, $\overline{A_C}$, were calculated for the period 2000-
475 2014 using the ESA CCI landcover product v2.0.7 (accessed 29th June 2017). ESA
476 CCI landcover classes were simplified into forested (classes 50, 60, 61, 62, 70, 71,
477 72, 80, 81, 82, 90, 100, 160, 170) and non-forested (classes 10, 11, 20, 30, 110,
478 130, 190) classes, the latter corresponding to cropland, grassland and urban land
479 uses. Then the area of 0.0028° pixels which were classified as forested in 2000 but
480 non-forested in 2014 was calculated. The forest loss due to land-use change
481 calculated from this dataset shows excellent consistency with the total forest loss
482 dataset based on Hansen *et al.*²¹, with only very few locations where the loss due
483 to land-use change is reported to be larger than the total (Suppl. Fig. 5).

484

485 Uncertainties in τ_0 due to the sample sizes in the forest loss data were estimated
486 through bootstrapping. In each 1° grid cell 1000 samples of $\overline{A_L}$ were created by
487 resampling with replacement the 0.01° grid cells designated as closed-canopy
488 forest. Uncertainties in $\overline{A_C}$ result from classification accuracy and scaling
489 differences between the Hansen *et al.*²¹ and ESA CCI datasets. Producer's accuracy
490 for the forest and non-forest classification in ESA CCI v2.0.7 is 92% and 78%
491 respectively, whilst the corresponding user's accuracy is 78% and 85%⁴⁵.
492 However, because we count the whole area of the pixel when an ESA CCI pixel
493 changes from forest to non-forest, and the CCI pixel area is *ca.* 100 times that of
494 Landsat, a scaling inaccuracy is induced, whereby the fraction of forest conversion

495 within the grid cell may be enough to cause a land-cover classification switch, but
496 substantially less than complete deforestation of the ESA pixel. To conservatively
497 account for classification and scaling errors we thus assume a 95% confidence
498 interval of $\pm 50\%$ in the forest conversion area values. For each 1° grid cell, 1000
499 samples of $\overline{A_C}$ were taken from a normal distribution defined by this confidence
500 interval. We crossed these 1000 samples of $\overline{A_C}$ with those from $\overline{A_L}$ to create a
501 matrix of 1×10^6 estimates of the denominator in Eq. 1. The 2.5th and 97.5th
502 percentiles of this matrix were then used to estimate the 95% confidence limits of
503 τ_0 . This resampling of the forest loss areas within the 1° pixel addresses the
504 uncertainty induced when the forest area in the pixel is relatively small, in which
505 case confidence in the fidelity of the space-for-time swap would be reduced. It also
506 accounts for classification errors if those errors are not correlated across the grid
507 cell. Hansen *et al.*²¹ report a tendency to underestimate forest loss by *ca.* 4% in the
508 tropics and overestimate it by *ca.* 6% in the temperate and boreal regions. These
509 classification biases are not captured in our uncertainty estimate, nor are
510 potential biases from $\overline{A_T}$ for which global quantification was not available. Based
511 on the available information, these biases are expected to be small and focused in
512 regions where the uncertainty is already assessed as being large (Suppl. Note 4;
513 Suppl. Fig. 8). Note that the capping of τ_0 at 1000 years often leads to very low
514 uncertainty for these grid cells, i.e. there is very high certainty that $\tau_0 > 1000$ years.
515 Calculated τ_0 is robust to subsampling of the 14 year observational period,
516 especially when the data series exceeds 10 years (Suppl. Fig. 6).

517

518 The resolution of ESA CCI landcover means it will have limited sensitivity to very
519 small-scale land-use conversions, such as have been recently reported in the

520 Amazon⁴⁶. However, given that our τ_0 values in the tropical evergreen forests are
521 very high, even in absence of the land-use correction (Suppl. Fig. 7) we expect the
522 influence on our results to be minimal.

523

524 The use of a 1° aggregation resolution represents a compromise between spatial
525 detail and sufficient area to make an effective space-for-time substitution.
526 Following the simplifying assumption that disturbance events are equally likely in
527 all locations in the grid cell, the maximum τ that we can expect to reliably quantify,
528 τ_m , for a given disturbance size, D , can be calculated as:

529
$$\tau_m = \frac{A_T \times t}{D}, (2)$$

530 where t is the total number of years sampled. The largest disturbance events are
531 generally fires, especially in the Canadian boreal region, for which the typical large
532 fire size is 6000 ha⁴⁷. Assuming a grid-cell area of 628 000 ha (60° latitude), a
533 forest coverage of 25% of grid-cell area (i.e. $A_T = 157\ 000$ ha) and a 14-year
534 sampling period, τ_m is 350 years at this scale. For smaller disturbances much
535 larger values of τ can be expected to be reliably captured. Substantial
536 undersampling of large rare events at 1° resolution would be expected to induce
537 scatter in our results, but Fig. 1 shows spatial coherence in variation of τ ,
538 suggesting any such under-sampling to have minimal effects. τ_0 was capped at
539 1000 years to avoid spuriously large values in grid cells with very infrequent
540 disturbance. The influence of this capping on simulated forest biomass is very
541 small (e.g. Fig. 3b).

542

543 **Forest type classification.** Forest types were classified based on ESA CCI
544 landcover v2.0.7. The mapping of landcover classes to the forest types used in this

545 analysis is shown in Suppl. Table 2. A map of these forest types is shown in Suppl.
546 Fig. 11. There is a small fraction of forest area that is not assigned to any of these
547 major forest classes, but is included in the global totals. Note that open canopy
548 forests (<50% canopy cover at 0.01° scale, see above) are not included in any of
549 the calculations herein. Forest type codes are: Tropical broadleaved evergreen
550 (TrBE), tropical broadleaved deciduous (TrBD), temperate broadleaved
551 evergreen (TeBE), temperate broadleaved deciduous (TeBD), needleleaved
552 evergreen (NE), needleleaved deciduous (ND), broadleaved-needleleaved mixed
553 forest (MX).

554

555 **Forest age dataset.** For cross comparison of spatial patterns in our results, we
556 used the Global Forest Age Dataset (GFAD v1.1)²², a forest stand age dataset
557 developed as part of the EU FP7 GEOCARBON project. It provides a distribution of
558 stand age and associated uncertainties in 10-year age bins up to an age of 140
559 years from a base year of 2010 on a 0.5° grid. The salient features are summarised
560 here and described in more detail in Pugh et al.⁴⁸. It combines datasets of forest
561 age distributions from the following forest inventories: United States Forest
562 Inventory and Analysis (v 5.1, state summaries, representative for the 2000s),
563 IIASA Russian Forests and Forestry Database (late 2000s), Canadian Forest
564 Inventory (CanFI, state summaries, 2001-2006), EFISCEN (Europe, 32 countries,
565 2000s), 6th National Forest Inventory (China, 1999-2003), and the national forest
566 inventories of Kazakhstan (2000s), New Zealand (2000s), Mongolia (2000s) and
567 Japan (2005). GFAD estimates forest age in tropical regions, where widespread
568 inventories are not available, by applying plant-functional-type-specific biomass-
569 age curves⁴⁹ to a large-scale forest biomass dataset⁵⁰.

570

571 **Forest modelling.** The LPJ-GUESS DGVM v4.0⁵¹ was used to calculate the effects
572 of τ on forest structure, dynamics and carbon cycling. LPJ-GUESS explicitly
573 simulates forest stand development and canopy structure divided among age
574 cohorts of trees co-occurring in patches representative of a wider landscape. Leaf
575 area to sapwood area ratio and maximum crown area for tropical evergreen tree
576 types were set to 10 000 and 130 m² respectively, in accordance with estimates
577 for tropical forests^{52,53}. Mortality and establishment are stochastic, with replicate
578 1000 m² patches simulated to capture the distribution of stands of different time-
579 since-last-disturbance across each grid cell. Stand-replacing disturbances are
580 simulated by clearing all trees in a patch and transferring their biomass stocks to
581 litter or out of the ecosystem (see below). We introduced a spatially-varying
582 stochastic disturbance frequency with an annual probability defined by $1/\tau$. In
583 order to allow LPJ-GUESS to simulate the closed-canopy forest area unrestricted
584 by the 25% cover threshold used to calculate τ_0 , the nearest-neighbour rule was
585 used to assign τ values to grid cells with less than 25% forest coverage. All forest-
586 type-level and global numbers are presented based on a 5% minimum forest
587 coverage mask at the grid-cell level to avoid overextrapolation of τ_0 to regions
588 with very low forest cover. The map in Fig. 2 is presented with a 25% closed-
589 canopy forest cover map for consistency with Fig. 1. Inclusion of τ_0 in LPJ-GUESS
590 improves the simulation of biomass compared to the disturbance settings in the
591 standard version of the model (Suppl. Fig. 12).

592

593 In the standard simulation setting, all cleared biomass is transferred to the litter
594 pools. For sensitivity simulations underlying ranges in Fig. 3d,e and Suppl. Fig. 10

595 two further setting types were employed to test the effect of the fate of disturbed
596 material. In the harvest sensitivity simulations fine root and leaf biomass, along
597 with 34% of woody biomass, are transferred to the litter, with the remaining
598 woody biomass being removed from the ecosystem, emulating product extraction.
599 The fire sensitivity simulations employ the interactive fire sub-model^{51,54} with a
600 local probability of fire occurrence (burnt area fraction) set to $1/\tau$, resulting in
601 most biomass carbon and some litter carbon being transferred to the atmosphere.
602 Stochastic processes use the same seed to ensure replication between simulations.
603 Simulations covered 1901-2014 using climate, atmospheric CO₂ mixing ratio and
604 N deposition as described in Le Quéré et al.⁵⁵. All model outputs shown are means
605 for 2001-2014. The standard simulations with τ_0 and $0.5\tau_0$ used 100 replicate
606 patches per grid cell. Simulations testing additional multiplicative perturbations
607 of τ (0.25, 2, 4) and using the confidence intervals of τ_0 used 10 replicate patches.
608 Differences at forest-type level were negligible between simulations with 10 and
609 100 patches.

610

611 Simulations used to create Fig. 3a used the standard model setup described above,
612 but the model was only run for the specified three grid cells. 100 simulations were
613 carried out for each grid cell using levels of τ from 10 years to 1000 years. A
614 second-order exponential equation of the form $B = ae^{b\tau} + ce^{d\tau}$ was fitted to these
615 simulations using the "fit" function of Matlab® 2014b.

616

617 **Sensitivity metric.** The metric is based upon differencing biomass between the
618 τ_0 and $0.5\tau_0$ simulations. The choice of a halving of τ_0 for the sensitivity metric
619 was informed by recent disturbance trends in Europe¹⁴, and is also similar to

620 changes in background mortality rates in the western U.S.A.⁵⁶. It thus represents
621 a reasonable sensitivity test. The sensitivity threshold τ_{crit} (Suppl. Table 1) was
622 estimated by first plotting against τ_0 the difference between biomass simulated
623 with $\tau = \tau_0$ and that simulated with $\tau = 0.5\tau_0$, (Fig. 3b, Suppl. Fig. 13). A second-
624 order exponential function was fitted to the data as for Fig. 3a. These fits were
625 carried out both globally and for individual forest types. 95% confidence intervals
626 for the fits were calculated using 1000 bootstrapped samples of the modelled grid
627 cells. $\tau_{crit,90}$ and $\tau_{crit,80}$ were taken as the intersection of the fitted line with a
628 difference of -10% and -20% biomass respectively (Suppl. Fig. 13), with
629 confidence intervals for τ_{crit} estimated using the confidence intervals of the fitted
630 lines. Scatter in the results is caused by the stochastic nature of the LPJ-GUESS
631 model, as well as variation in climate across the domain. The 90% biomass
632 threshold is consistent with recent work on the recovery of forest biomass³³ and
633 with the character of the curve in Fig. 3b.

634

635 The area of forest in each sensitivity regime (Fig. 3c) was created by comparing τ_0
636 for each grid cell with the τ_{crit} for the forest type to which that grid cell was
637 assigned. Uncertainty in the areas of the regimes (Main text) was calculated based
638 on the 95% confidence intervals of τ_0 . For forest grid cells not classified by one of
639 the seven forest types, not enough data points existed to make a reliable fit to
640 calculate τ_{crit} . Therefore the global mean τ_{crit} was used to determine the sensitivity
641 regime. Fig. 3d,e shows the difference in biomass and soil carbon density between
642 model sensitivity simulations with different multiplicative factors of τ (see above)
643 averaged across the area of forest allocated to each sensitivity class. Variation in

644 response across the vulnerability classes is much less than that between them
645 (Suppl. Fig. 9).

646

647 **Empirical cross-checks.** For cross-checking of biomass carbon turnover flux due
648 to disturbance (F_d) we used the GEOCARBON global biomass dataset²⁷⁻²⁹, in which
649 biomass values are based on linking satellite-based LIDAR and radar observations
650 with ground-based forest plot data. We replaced values for northern forests with
651 those of Thurner et al.³⁰ due to the latter's more sophisticated approach to linking
652 satellite-based radar observations with above- and below-ground biomass in
653 these regions. Below-ground biomass for the GEOCARBON dataset was estimated
654 following Saatchi et al.⁵⁰ and a biomass to carbon conversion factor of 0.5 was
655 assumed. We then multiplied the carbon content of this observationally-based
656 total biomass dataset by $1/\tau_0$ to calculate F_d . Cross-checking the fraction of total
657 turnover due to disturbance (T_{frac}) involved making the assumption that NPP and
658 turnover fluxes are not drastically out of equilibrium, and therefore NPP must be
659 broadly equal to the turnover flux of biomass carbon in the multi-annual mean.
660 Annual mean NPP over the period 2001-2010 was calculated from Zhao and
661 Running⁵⁷. T_{frac} was then approximated as F_d/NPP . Fire emissions from the GFED
662 dataset³² were calculated by summing the boreal, temperate and tropical forest
663 wildfire emissions, excluding the savannah category, which does not fit our
664 definition of closed-canopy forest. The mask of at least 5% forest cover per grid
665 cell was applied to all these cross-check calculations as above.

666

667 **Data availability**

668

669 Calculations of τ_0 , data from the model simulations and the forest mask used are
670 available from <https://dataguru.lu.se/app#PughDisturbance2019> (dois:
671 10.18161/disturbance_tauo.201905, 10.18161/disturbance_lpj-guess.201905,
672 10.18161/disturbance_forestmask.201905). GFAD v1.1 was obtained from
673 PANGAEA²², and the Global Forest Change 2000-2014 v1.2 forest loss product from
674 [https://earthenginepartners.appspot.com/science-2013-global-
675 forest/download_v1.2.html](https://earthenginepartners.appspot.com/science-2013-global-forest/download_v1.2.html). The ESA CCI Landcover v2.0.7 was obtained from
676 <http://maps.elie.ucl.ac.be/CCI/viewer/>.

677

678 **Code availability**

679

680 Matlab code for the data analysis herein is available from GitHub,
681 <https://github.com/pughtam/GlobalDist>. Source code for LPJ-GUESS v4.0 can be
682 obtained on request through Lund University, see web.nateko.lu.se/lpj-guess.

683

684 **Methods References**

685

- 686 45. ESA. Land Cover CCI Product User Guide Version 2.0. (ESA,
687 2017). [http://maps.elie.ucl.ac.be/CCI/viewer/download/ESACCI-LC-Ph2-
688 PUGv2_2.0.pdf](http://maps.elie.ucl.ac.be/CCI/viewer/download/ESACCI-LC-Ph2-PUGv2_2.0.pdf)
- 689 46. Kalamandeen, M. et al. Pervasive Rise of Small-scale Deforestation in
690 Amazonia. *Sci. Rep.* **8**, 1600 (2018).
- 691 47. de Groot, W. J. et al. A comparison of Canadian and Russian boreal forest
692 fire regimes. *For. Ecol. Manage.* **294**, 23–34 (2013).

- 693 48. Pugh, T. A. M. et al. Role of forest regrowth in global carbon sink
694 dynamics. *Proc. Natl. Acad. Sci. U. S. A.* **116**, 4382–4387 (2019).
- 695 49. Marin-Spiotta, E., Cusack, D. F., Ostertag, R. & Silver, W. L. Trends in above
696 and belowground carbon with forest regrowth after agricultural
697 abandonment in the neotropics. in *Post-agricultural succession in the*
698 *Neotropics* (ed. Myster, R. W.) (Springer, New York, 2008).
- 699 50. Saatchi, S. S. et al. Benchmark map of forest carbon stocks in tropical
700 regions across three continents. *Proc. Natl. Acad. Sci.* **108**, 9899–9904
701 (2011).
- 702 51. Smith, B. et al. Implications of incorporating N cycling and N limitations
703 on primary production in an individual-based dynamic vegetation model.
704 *Biogeosciences* **11**, 2027–2054 (2014).
- 705 52. Herwitz, S., Slye, R., Erwitz, S. T. R. H. & Lye, R. O. E. S. Long-term
706 survivorship and crown area dynamics of tropical rain forest canopy
707 trees. *Ecology* **81**, 585–597 (2000).
- 708 53. Calvo-Alvarado, J. C., McDowell, N. G. & Waring, R. H. Allometric
709 relationships predicting foliar biomass and leaf area:sapwood area ratio
710 from tree height in five Costa Rican rain forest species. *Tree Physiol.* **28**,
711 1601–1608 (2008).
- 712 54. Thonicke, K., Venevsky, S., Sitch, S. & Cramer, W. The role of fire
713 disturbance for global vegetation dynamics: coupling fire into a Dynamic
714 Global Vegetation Model. *Glob. Ecol. Biogeogr.* **10**, 661–677 (2001).
- 715 55. Le Quéré, C. et al. Global Carbon Budget 2016. *Earth Syst. Sci. Data* **8**, 605–
716 649 (2016).

- 717 56. van Mantgem, P. J. et al. Widespread increase of tree mortality rates in the
718 western United States. *Science* **323**, 521–524 (2009).
- 719 57. Zhao, M. & Running, S. W. Drought-Induced Reduction in Global
720 Terrestrial Net Primary Production from 2000 Through 2009. *Science*
721 **329**, 940–944 (2010).
- 722